Theoretical Study of the anti-NCP Molecular Mechanism of Traditional Chinese Medicine Lianhua-Qingwen Formula (LQF)

Cheng-hao Ye[1, #], Mei-na Gao[2, 3 #], Wang-qiang Lin[1], Kun-qian Yu[3], Peng Li[4], and Guang-hui Chen[1, *]

1. Department of Chemistry and Key Laboratory for Preparation and Application of Ordered Structural Materials of Guangdong Province, Shantou University, Guangdong Province, 515063, China
2. Nanjing University of Chinese Medicine, Jiangsu Province, 210029, China
3. State Key Laboratory of Drug Research, Shanghai Institute of Materia Medica, Chinese Academy of Sciences, Shanghai, 201203, China
4. School of Life and Health Sciences, The Chinese University of Hong Kong, Shenzhen, Guangdong Province, 518172, China

# These authors contributed equally to this work

* Corresponding author: Guang-hui Chen (ghchen@stu.edu.cn)

Abstract

Due to the good clinical efficacy in treating Novel Coronavirus Pneumonia (NCP) resulted from SARS-CoV-2, as the traditional Chinese medicine(TCM) prescription, Lianhua Qingwen Formula (LQF) was composed into the Diagnosis and Treatment Programs of 2019 New Coronavirus Pneumonia (from fourth to seventh editions) formulated by the National Health Commission of China. Aiming to prevent and treat viral influenza, LQF was patented from 2003 in China, and passed the Phase II clinical trial by FDA in the United States in 2015. However, the molecular mechanism of LQF anti SARS-CoV-2 pneumonia is still not clear. It is shown that the docking scores of three components in LQF including Rutin, Forsythoside E, and Hyperoside to main protease of SARS-CoV-2 are very large as -9.1, -9.0 and -8.7 kcal/mol, respectively, which are even better than those of Lopinavir at -7.3 kcal/mol. Importantly, the binding modes between active compounds and protein were verified via molecular dynamics (MD) simulation and calculation all the binding free energies at MM-PBSA level. Note that these donor-acceptor systems were stabilized by non-polar interactions including hydrogen bonds and hydrophobic interactions. At last, from the constructed component-target-pathway network, it is shown that the components in LQF are related important pathways to improve the human immunity such as T cell, B cell receptor signaling, natural killer cell mediated cytotoxicity, as well as anti-inflammatory pathways including Fc epsilon RI, ErbB, MAPK signaling and so on. The present investigation represents the first report on the molecular mechanism of LQF as NCP inhibitor.

Keywords: SARS-CoV-2; Inhibitor; Lianhua-Qingwen Formula; CADD; Network pharmacology.

1. Introduction

From December of 2019, there was an outbreak of new pneumonia resulting from new coronavirus named as SARS-CoV-2 in Wuhan city of China[1]. The syndrome of new coronavirus pneumonia (NCP) includes fever, cough, and hypodynamic with fatality to some extent[2-3]. The World Health Organization (WHO) declared the SARS-CoV-2 viral disease has been swept into at least 114 countries and led to death of more than 4,000 people. Drug development for treating SARS-CoV-2 is urgent due to the rapid spread of NCP. It should be noted that TCM has a long history for the prevention and treatment of various diseases in China by targeting and modulating multiple disease related pathways with multiple effective components[4]. After strict therapeutic effect evaluation, Lianhua Qingwen Formula (LQF) was composed into the Diagnosis and Treatment Programs of 2019 New Coronavirus Pneumonia formulated by the National Health Commission of China[5-8]. Nowadays, although TCMs are widely used for prevention and treatment of viral pneumonia in China[9], there still some doubts on how the TCM works and what is the effective compounds.

As we know that during the period of spreading of SARS-CoV to MERS-CoV, the computer-aided drug design (CADD) plays an important role to discover the CoV inhibitors[10]. In addition, network pharmacology has been recently developed as a powerful tool to explore the relation among drug compoments, targets, and pathways toward a certain disease[11-13] . Therefore, in this work we tested the effect of Chinese patent medicine of LQF on anti-SARS-CoV-2 by virtual screening at first. Secondly, based on network pharmacology, we tried to construct a component-target-pathway network between the LQF and viral pneumonia to explain the mechanism of anti-inflammatory and human immunity.

Aiming to prevent and treat viral influenza, the LQF came from two well-known TCM prescriptions Maxing-Shigan-Tang and Yinqiao-San, was patented from 2003 in China, and passed the Phase II clinical trial by FDA in the United States in 2015[14-15]. The LQF contains 11 herbs including Radix Isatidis (Banlangen), Fructus Forsythiae (Lianqiao), Flos Lonicerae Japonicae (Jinyinhua), Rhizoma Dryopteridis Crassirhizomatis (Mianmaguanzhong), Herba Ephedrae (Mahuang), Semen Armeniacae Amarum (Kuxingren), Herba Houttuyniae (Yuxingcao), Herba Pogostemonis (Guanghuoxiang), Radix et Rhizoma Rhodiolae Crenulatae (Hongjingtian), Radix et Rhizoma Rhei (Dahuang) and Radix et Rhizoma Glycyrrhizae (Gancao) and a mineral medicine, Gypsum Fibrosum (Shigao) as well as menthol. Duan, etc proved Lianhua Qingwen Capsule has the same effect as Oseltamivir on treating influenza A (H1N1) virus infections[16]. LQF had been developed for the analysis of absorbed components in SD rat plasma after oral administration by UPLC-Q-TOF-MS method and total 21 main chemical components[17]. In this study, we focused on the inhibiting effect on NCP of the molecular structures of 21 compounds in LQF and lopinavir as plotted in Figure 1. Note that lopinavir is suggested in treating mild cases of SARS-CoV-2 infection by National Health Commission of China. Based on the mixed compounds, we propose that some of the LQF gradients can inhibit the SARS-CoV-2 reproduction and enhance the immunity efficiently.

2. Computational methods

Molecule docking. The component small molecules of LQF were optimized at B3LYP-D3/6-31G(d, p) level of theory with Gaussian 16 package at first[18]. Just like the SARS-CoV[14], taking the main protease (Mpro) of SARS-CoV-2 from PDB bank (PDB code: 6LU7) as target[19], we tried to dock it with the 21 components in LQF, respectively, by using AutoDock Vina program[20]. The possible docking conformations and binding modes were predicted in the grid of protein. In this study, a grid

of 40 × 40 × 40 points in the x, y, and z-axis directions was built and the center of grid was x = -18.954, y = 16.918, z = 68.850 with the exhaustiveness of 20.

Molecular dynamics (MD) simulation. After docking, the complex systems with the top three highest docking score were submitted to 20 ns of MD simulations so as to check their stability inside the binding pocket of the main protease in SARS-CoV-2 and verify which residues interact with the ligands. All of the complexes were prepared after molecular docking and then subjected to MD simulation in a periodic boundary condition using the GROMACS 2018.4 software package[21-22] with TIP3P water model[23] (Supplementary table 1). The Amber 99 sb-ILDN force field was applied to describe the receptors, ligands, ions and water[24]. ACPYPE[25] is a tool based on Python programming language to generate parameters and topologies for ligands with ANTECHAMBER, using GAFF force field[26]. To keep each system electrically neutral, sodium and chloride ions were added to substitute for water molecules to produce a solvent box of 0.15 M NaCl. Initially, the complex systems were relaxed with conjugate gradient energy minimization to prevent from steric clashes or incorrect geometry. Then the restrained complex systems were simulated with position-restrained MD within 100 ps, in case of drastic rearrangement during equilibration. At last, 20 ns MD simulation of products were performed at 300 K under the NPT ensemble.

Decomposition of binding free energy between ligand and residue. The binding free energies were calculated by g_mmpbsa program[27-28] using the MM-PBSA method[29-30]. The 500 snapshots of last 5 ns MD trajectories were chosen to calculate the binding energy and interaction decomposition. The MM-PBSA method can be conceptually summarized as:

$$\Delta G_{bind} = \Delta G_{complex} - [\Delta G_{protein} + \Delta G_{lig}] \quad (1)$$

$$\Delta G_{bind} = \Delta H - T\Delta S \quad (2)$$

where ΔH of the system consists of the enthalpy changes in the gas phase on complex formation (ΔE_{MM}) and the solvated free energy contribution (ΔG_{sol}), while -TΔS refers to the entropy contribution to the binding. Note that the entropy differences should be very small, thus the calculation of the solute entropy term was ignored in present study, and Eq. (2) can be transformed into Eq. (3):

$$\Delta G_{bind} = \Delta E_{MM} + \Delta G_{sol} \quad (3)$$

where ΔE_{MM} is the summation of van der Waals (ΔE_{wdW}) and the electrostatic (ΔE_{ele}) interaction energies.

$$\Delta E_{MM} = \Delta E_{vdW} + \Delta E_{ele} \quad (4)$$

In addition, ΔG_{sol}, in Eq. (3) which signifies the solvation free energy, can be calculated as the summation of electrostatic component, the polar part ($\Delta G_{PB,sol}$) and nonpolar component ($\Delta G_{nonpolar,sol}$), are shown in Eq. (5). The nonpolar contribution to the free energy was calculated via γSASA, where SASA was the solvent-accessible surface area, γ was 0.0227 kcal/mol/Å^2, and the solvent-probe radius for SASA was 1.4 Å. Note that the offset of SASA calculation was 3.8493 kJ/mol.

$$\Delta G_{sol} = \Delta G_{PB,sol} + \Delta G_{nonpolar,sol} \quad (5)$$

Construction of component-target-pathway network. Network pharmacology analysis is a way of representing datasets emphasizing the relationships between nodes[31-32]. The active components, which have been detected in the rat plasma[17], were used as keywords to search the related potential targets from Traditional Chinese Medicine System Pharmacology Database and Analysis Platform

(TCMSP)[33]. Totally 1080 virus pneumonia related proteins were collected from GeneCard Database[34], whose relevance scores were over 5. Intersection of targets were uploaded in DAVID database[35] using the Functional Annotion Tool to obtain relevant targets and KEGG-Pathways. The related targets and pathways were used as input to the software Cytoscape[36] to construct the component-target-pathway network. The degree of a node is the number of edges connecting nodes depicting the probability distribution of these degrees over the whole network. Note that local based method considers the direct neighborhood of a vertex. Given a node v, $N(v)$ denotes the collection of its neighbors[37]. Node degree (Deg) is calculated as follow:

$$Deg(v)=|N(v)| \tag{6}$$

3. Results

3.1 The interaction between components of LQF and main protease

We docked 21 compounds into main protease of SARS-CoV-2 using a flexible docking procedure. The top three highest compounds were Rutin, Hyperoside and Forsythoside E, which bind with the main protease at -9.1, -9.0 and -8.7 kcal/mol, respectively, and the reported prescription of anti-SARS-CoV-2, Lopinavir only reached -7.3 kcal/mol. Rutin directly interacts with residues Leu141, Ser144, His163 and Asp187 as plotted in Figure 2a. Forythoside E formed excellent hydrogen bonds with residues Leu141, Ser144, Cys145, His 164, Glu166, Glu189, Thr190 as plotted in Figure 2b. Hyperoside interacts with Mpro in the Thr26, Ser144, Cys145, Glu166 and Asp187 as plotted in Figure 2c, where glycosyl moiety of Hyperoside form hydrogen bonds with residues Ser144, Cys145 and Glu166 directly. On the contrary, Lopinavir provides only hydrogen atoms on nitrogen atoms of imino to form hydrogen bonds with residue Glu166 and Gln189 as plotted in Figure 2d. According the

docking scores, we found that not all the ingredients in LQF can inhibit the main protease of SARS-CoV-2. The top-ranked poses of compounds were arranged by docking score as collected in Table 1.

3.2 Binding mode verification in MD simulation

In order to explore whether the above three compounds in LQF including Forsythoside E, Rutin, and Hyperoside could bind with the pocket of main protease of SARS-CoV-2 stably, we also calculated the root-mean-square deviation (RMSD) between ligands, including lopinavir, and Cα atoms of protein by molecular dynamic simulation. After 20 ns stimulation we found that all these four compounds attain an equilibrium, but Forsythoside E, Rutin, and Hyperoside arrived more quickly than Lopinavir. The RMSD results with smooth fluctuation showed the ligands in the binding pockets were energetically stable, which can be recognized the compounds tend to interact with the potential binding pocket in SARS-CoV-2 main protease as shown in Figure 3a and Figure S1. This means that the three components in LQF combine with Mpro more easily than Lopinavir. According to the binding free energies at the MM-PBSA level, we found that Forsythoside E, Rutin and Hyperoside were stabilized by van der Waals and electrostatic interactions as plotted in Figure 3b. Hyperoside-Mpro complex showed the lowest energy among these systems while Lopinavir-Mpro corresponded to the highest energy system. The calculated free energy proved that non-polar interactions including hydrogen-bonds and hydrophobic interactions contributed to the binding energy most between Hyperoside and Mpro of SARS-CoV-2 as listed in Supplementary table 2.

The hydrogen bonds play a significant role in maintaining the interaction between the protein and ligand[38]. Hydrogen bonds between each ligand and protein presented in the whole last 5 ns simulation were confirmed with highly contributing residues, such as Met49 and Met 165 in Lopinavir complex.

Hyperoside-Mpro, Rutin-Mpro and Forsythoside E-Mpro complexes possessed the maximum number of intermolecular hydrogen bonds at six over the simulation period, compared with only two hydrogen bonds in the Lopinavir-Mpro complex as plotted in Figure 3c. Meanwhile, the lifetime of hydrogen bonds were computed as well, the hydrogen bonds in complex of Rutin, Forysthoside E, Hyperoside and Lopinavir had apparently longer lifetime at 42.4, 32.1, 28.2 and 26.0 ps, respectively, as listed in Supplementary table 3. So, Rutin, Forysthoside E and Hyperoside have higher affinity to main protease of SARS-CoV-2 according to their lower binding energies and more hydrogen bonds with longer lifetime. It is shown that the combination of Hyperoside with Mpro is more stable than those of Lopinavir, Rutin, and Forysthoside E as well.

Then we calculated the RMSF of above four compound-Mpro systems, respectively. The fluctuations of lines were very similar, indicating that the binding modes of the ligands are in same pattern as plotted in Figure 3d. It is shown that Forsythoside E was located in the pocket around His41, Met165, Glu166, Asp187, Arg188, Gln189, Thr190 and Gln192 with lower binding free energies of -45.76 kcal/mol as plotted in Figure 4a. Rutin tended to interact mainly with residues His41, Met49, Gly143, Ser144, Cys145, Met165, Glu166 and Glu189 because of the greater binding free energy contribution of them as shown in Figure 4b. Among the results of the top three complexes, Hyperoside performed the highest absolute value of binding free energy of -48.41 kcal/mol which could be decomposed into ΔE_{vdW} (-54.20 kcal/mol), ΔE_{ele} (-39.15 kcal/mol), ΔE_{PB} (49.83 kcal/mol) and $\Delta E_{nonpolar}$ (-4.89 kcal/mol) (Supplementary table 2). The Hyperoside mainly interacted with residues Thr26, Met49, Tyr54, Gly143, Cys145, Met165, Asp187 and Gln189 with energies at -3.88, -2.97, -1.95, -3.87, -2.55, -3.09, -3.09 and -4.97 kcal/mol, respectively, as shown in Figure 4b, which provided

greater contribution in Hyperoside-MPro complex system via van der Waals and electrostatic interactions. Note that these residues participated in the complex binding apparently as plotted in Figure 4c. The calculated free energy proved that van der Waals and electrostatic interactions contributed most to the binding between Hyperoside and SARS-CoV-2 main protease. In the Rutin-Mpro complex, the binding free energy was also very low of -47.67 kcal/mol as listed in Supplementary table 2. Note that the absolute values of binding free energies of these three compounds combining with main protease are much larger than that of Lopinavir. The binding energy of Lopinavir was -34.42 kcal/mol and could be decomposed into ΔE_{vdW} (-46.99 kcal/mol), ΔE_{ele} (-15.04 kcal/mol), ΔE_{PB} (39.07 kcal/mol) and $\Delta E_{nonpolar}$ (-5.47 kcal/mol), respectively, indicating that Lopinavir was bound in the pocket around residues His41, Met49, Gly143, Ser144, Cys145, Met165, Glu166 and Gln189, respectively, as plotted in Figure 4d. Therefore, we concluded that the critical residues were Met165, Gln189, Cys145, Asp187.

3.3 Ingredient-target-pathway network analysis

Network analysis. Severe SARS-CoV-2 infection can rapidly activate pathogenic T cells and produce granulocyte-macrophage colony, with some important Cytokine Response Patterns, and the high-levels of proinflammatory cytokines including IL-2, IL-6, IL-7, IL-10, G-CSF, IP-10, MCP-1, MIP-1A, VEGF and TNFα were observed in the SARS-CoV-2 severe cases[39-40]. As shown in Figure 5, we found that the relative targets of 21 compounds of LQF interact with signaling pathways of inflammation and immunity, such as VEGF signaling pathway[41], Toll-like receptor signaling pathway[42], T cell receptor signaling pathway[43], Fc epsilon RI signaling pathway[44], B cell receptor signaling pathway[45], ErbB signaling pathway[46], MAPK signaling pathway[47], natural killer cell mediated cytotoxicity[48], JAK-

STAT signaling pathway[49], complement and coagulation cascades[50]. We collected 1080 virus pneumonia-related proteins from GeneCard Database, whose relevance scores were over 5. The 42 active components' genes were collected from TCMSP database overall[51], and the intersection of two parts contains 37 genes. Then we collected 79 related targets and 10 pathways of inflammatory and immunity via uploading the 37 genes to DAVID database[35]. Formononetin, Rutin, Emodin 8-O-β-D-glucoside, Hyperoside, Loganic acid, Salidroside in the LQF connect potential targets directly which are relevant to anti-inflammatory and immunity mechanisms (Supplementary table 4 and 5). Thus, Formononetin, Rutin, Emodin 8-O-β-D-glucoside, Hyperoside, Loganic acid, Salidroside, are key components which are beneficial in preventing viral infection because they acquire higher node degrees of compounds in ingredient-target-pathway network. The node degrees of Formononetin, Rutin and Emodin 8-O-β-D-glucoside are over 10 while the average of the node degree is only 2.92 (Supplementary table 6). The node degrees of T cell receptor signaling pathway, MAPK signaling pathway and Toll-like receptor signaling pathway are over 4 while the average of the node degree is 3.80 (Supplementary table 7). The component-target-pathway network includes 111 nodes along with 487 edges as plotted in Figure 5, which interprets interactions among compounds, targets and pathways. These candidate targets are collected from databases and have been proved to be affected by LQF's components.

Main effective component identification and validation. The viral pneumonia involves multiple processes such as infection, inflammation, immunity, coagulation, tissue damage and genetic polymorphisms[52]. It has been reported that Emodin, Formononetin, Amygdalin from TCM can cure the viral pneumonia through regulating the immunity[53-56]. Salidroside reduced tumor necrosis factor-

α (TNF-α), interleukin-6 (IL-6) interleukin-1β (IL-1β) secretions and downregulated LPS-induced nuclear transcription factor-κB (NF-κB) DNA-binding activation and ERK/MAPKs signal transduction pathways[57-58]. These effects of salidroside may be of potential importance in the treatment of inflammation-mediated endotoxemia. Formononetin significantly inhibited TNF-α, IL-1, IL-6, monocyte chemoattractant protein-1 (MCP-1), and activated the T-cell cytoplasmic 1 signaling pathway to increase the expression and secretion of T cells[59]. Rutin may be a promising modulator in inflammation and hepatotoxicity via down regulating the levels of inflammatory markers like TNF-α, IL-6 and expressions of p38-MAPK, NFκB, i-NOS and COX-2[60-61]. Emodin 8-O-β-D-glucoside inhibited the elevated expression levels of tumor necrosis factor-α (TNF-α), interleukin (IL)-1β and IL-10 in the LPS-stimulated Raw 264.7 cells, indicating Emodin 8-O-β-D-glucoside effectively suppressed LPS-induced inflammatory cytokine secretion[62].

Therefore, Salidroside, Amygdalin, Sweroside, Emodin 8-O-β-D-glucoside, Formononetin, Chlorogenic acid, Hyperoside and Rutin count more than the other candidate components in the network of 10 signaling pathways of inflammation and immunity as listed in Table 2. The results of drug-target-pathway network correspond to the experimental results indicate that the active compounds in LQF have explicit anti-inflammatory effect and could activate T-cell cytoplasmic to increase the expression of T cells and reduce the symptoms of SARS-CoV-2 according to network pharmacology analysis.

4. Conclusion

Although LQF has been found with good clinical efficacy in treating Novel Coronavirus Pneumonia (NCP) resulted from SARS-CoV-2, the molecular mechanism of LQF anti SARS-CoV-2 pneumonia

is still not clear. In this work, we have investigated the effect of LQF anti-SARS-CoV-2 with computer-aided drug design (CADD) of virtual screening as well as the mechanism of anti-inflammatory and immunity towards virus pneumonia with network pharmacology. The docking scores revealed that Rutin, Forsythoside E, and Hyperoside could reach more stable conformation than Lopinavir. After further MD simulation and MM-PBSA calculation of binding free energies, it is shown that Hyperoside may be the most possible inhibitor to main protease of SARS-CoV-2 with hydrogen-bonds and hydrophobic interactions. In summary, LQF could reduce symptoms of SARS-CoV-2 pneumonia via synergistic effects including antiviral and anti-inflammatory which are activated by the crucial molecules according to the network pharmacology analysis. Therefore, LQF has not only anti-viral effect but also anti-inflammatory and immunity mechanisms. This is also consistent with the character of TCM, i.e., comprehensive therapy complex disease with multi components, multi targets, and multi pathways.

5. Acknowledgements

This work was supported by the National Key R & D Program of China (2016YFB0201700), the National Science and Technology Major Projects for "Major New Drugs Innovation and Development" (2018ZX09711003-003-005), and the Strategic Priority Research Program of the Chinese Academy of Sciences (XDC01040100).

References

1. Hui, D. S.; I Azhar, E.; Madani, T. A.; Ntoumi, F.; Kock, R.; Dar, O.; Ippolito, G.; Mchugh, T. D.; Memish, Z. A.; Drosten, C., The continuing 2019-nCoV epidemic threat of novel coronaviruses to global health—The latest 2019 novel coronavirus outbreak in Wuhan, China. *International Journal of Infectious Diseases* **2020,** *91*, 264-266.

2. Fisher, D.; Heymann, D., Q&A: The novel coronavirus outbreak causing COVID-19. *BMC medicine* **2020,** *18* (1), 1-3.

3. KANNAN, S.; ALI, P. S. S.; SHEEZA, A.; HEMALATHA, K., COVID-19 (Novel Coronavirus 2019)–recent trends. *European Review for Medical and Pharmacological Sciences* **2020,** *24*, 2006-2011.

4. Zimmermann, G. R.; Lehar, J.; Keith, C. T., Multi-target therapeutics: when the whole is greater than the sum of the parts. *Drug discovery today* **2007,** *12* (1-2), 34-42.

5. National Health Commission of China, Notice on the issuance of a program for the diagnosis and treatment of novel coronavirus (2019-nCoV) infected pneumonia (trial sixth edition). **2020**.

6. National Health Commission of China, Notice on the issuance of a program for the diagnosis and treatment of novel coronavirus (2019-nCoV) infected pneumonia (trial seventh edition). **2020**.

7. National Health Commission of China, Notice on the issuance of a program for the diagnosis and treatment of novel coronavirus (2019-nCoV) infected pneumonia (trial fourth edition). **2020**.

8. National Health Commission of China, Notice on the issuance of a program for the diagnosis and treatment of novel coronavirus (2019-nCoV) infected pneumonia (trial fifth edition). **2020**.

9. Lin, L.; Yan, H.; Chen, J.; Xie, H.; Peng, L.; Xie, T.; Zhao, X.; Wang, S.; Shan, J., Application of metabolomics in viral pneumonia treatment with traditional Chinese medicine. *Chinese medicine* **2019,** *14* (1), 8.

10. Zumla, A.; Chan, J. F.; Azhar, E. I.; Hui, D. S.; Yuen, K.-Y., Coronaviruses—drug discovery and therapeutic options. *Nature reviews Drug discovery* **2016,** *15* (5), 327.

11. Hopkins, A. L., Network pharmacology. *Nature biotechnology* **2007,** *25* (10), 1110-1111.

12. Hopkins, A. L., Network pharmacology: the next paradigm in drug discovery. *Nature chemical biology* **2008,** *4* (11), 682.

13. Liang, X.; Li, H.; Li, S., A novel network pharmacology approach to analyse traditional herbal formulae: the Liu-Wei-Di-Huang pill as a case study. *Molecular BioSystems* **2014,** *10* (5), 1014-1022.

14. Anand, K.; Ziebuhr, J.; Wadhwani, P.; Mesters, J. R.; Hilgenfeld, R., Coronavirus main proteinase (3CLpro) structure: basis for design of anti-SARS drugs. *Science* **2003,** *300* (5626), 1763-1767.

15. YILING, W., Anti-virus Chinese medicine composition and preparation process thereof. **2003,** *CN1483463A.* .

16. Duan, Z.-p.; Jia, Z.-h.; Zhang, J.; Shuang, L.; Yu, C.; Liang, L.-c.; Zhang, C.-q.; Zhang, Z.; Yan, S.; Zhang, S.-q., Natural herbal medicine Lianhuaqingwen capsule anti-influenza A (H1N1) trial: a randomized, double blind, positive

controlled clinical trial. *Chinese medical journal* **2011,** *124* (18), 2925-2933.

17. Yu, H.; Jia, W.; Liu, J.; Zhu, Y.; Wang, C.; Analysis of absorbed components in rat plasma after oral administration of Lianhua Qingwen capsules by UPLC-Q-TOF-MS. Tianjin Journal of Traditional Chinese Medicine, 2016. 33: 756-759.

18. Frisch, M.; Trucks, G.; Schlegel, H.; Scuseria, G.; Robb, M.; Cheeseman, J.; Scalmani, G.; Barone, V.; Petersson, G.; Nakatsuji, H., Gaussian 16 revision a. 03. 2016; gaussian inc. *Wallingford CT* **2016,** *2* (3), 4.

19. Liu, X.; Zhang, B.; Jin, Z.; Yang, H.; Rao, Z., The Crytal Structure of 2019-NCoV Main Protease in Complex with an Inhibitor N3. *RCSB Protein Data Bank* **2020**.

20. Vina, A., Improving the speed and accuracy of docking with a new scoring function, efficient optimization, and multithreading Trott, Oleg; Olson, Arthur J. *J. Comput. Chem* **2010,** *31* (2), 455-461.

21. Berendsen, H. J.; van der Spoel, D.; van Drunen, R., GROMACS: a message-passing parallel molecular dynamics implementation. *Computer physics communications* **1995,** *91* (1-3), 43-56.

22. Lindahl, E.; Hess, B.; Van Der Spoel, D., GROMACS 3.0: a package for molecular simulation and trajectory analysis. *Molecular modeling annual* **2001,** *7* (8), 306-317.

23. Mark, P.; Nilsson, L., Structure and dynamics of the TIP3P, SPC, and SPC/E water models at 298 K. *The Journal of Physical Chemistry A* **2001,** *105* (43), 9954-9960.

24. Lindorff-Larsen, K.; Piana, S.; Palmo, K.; Maragakis, P.; Klepeis, J. L.; Dror, R. O.; Shaw, D. E., Improved side-chain torsion potentials for the Amber ff99SB protein force field. *Proteins: Structure, Function, and Bioinformatics* **2010,** *78* (8), 1950-1958.

25. Da Silva, A. W. S.; Vranken, W. F., ACPYPE-Antechamber python parser interface. *BMC research notes* **2012,** *5* (1), 367.

26. Wang, J.; Wolf, R. M.; Caldwell, J. W.; Kollman, P. A.; Case, D. A., Development and testing of a general amber force field. *Journal of computational chemistry* **2004,** *25* (9), 1157-1174.

27. Baker, N. A.; Sept, D.; Joseph, S.; Holst, M. J.; McCammon, J. A., Electrostatics of nanosystems: application to microtubules and the ribosome. *Proceedings of the National Academy of Sciences* **2001,** *98* (18), 10037-10041.

28. Kumari, R.; Kumar, R.; Consortium, O. S. D. D.; Lynn, A., g_mmpbsa□ A GROMACS tool for high-throughput MM-PBSA calculations. *Journal of chemical information and modeling* **2014,** *54* (7), 1951-1962.

29. Hou, T.; Wang, J.; Li, Y.; Wang, W., Assessing the performance of the MM/PBSA and MM/GBSA methods. 1. The accuracy of binding free energy calculations based on molecular dynamics simulations. *Journal of chemical information and modeling* **2011,** *51* (1), 69-82.

30. Genheden, S.; Ryde, U., The MM/PBSA and MM/GBSA methods to estimate ligand-binding affinities. *Expert opinion on drug discovery* **2015,** *10* (5), 449-461.

31. Berger, S. I.; Iyengar, R., Network analyses in systems pharmacology. *Bioinformatics* **2009,** *25* (19), 2466-2472.

32. Gomez-Verjan, J.; Ramírez-Aldana, R.; Pérez-Zepeda, M.; Quiroz-Baez, R.; Luna-López, A.; Robledo, L. G., Systems biology and network pharmacology of frailty reveal novel epigenetic targets and mechanisms. *Scientific reports* **2019,** *9* (1), 1-12.

33. Ru, J.; Li, P.; Wang, J.; Zhou, W.; Li, B.; Huang, C.; Li, P.; Guo, Z.; Tao, W.; Yang, Y., TCMSP: a database of systems pharmacology for drug discovery from herbal medicines. *Journal of cheminformatics* **2014,** *6* (1), 13.

34. Stelzer, G.; Rosen, N.; Plaschkes, I.; Zimmerman, S.; Twik, M.; Fishilevich, S.; Stein, T. I.; Nudel, R.; Lieder, I.; Mazor, Y., The GeneCards suite: from gene data mining to disease genome sequence analyses. *Current protocols in bioinformatics* **2016,** *54* (1), 1.30. 1-1.30. 33.

35. Dennis, G.; Sherman, B. T.; Hosack, D. A.; Yang, J.; Gao, W.; Lane, H. C.; Lempicki, R. A., DAVID: database for annotation, visualization, and integrated discovery. *Genome biology* **2003,** *4* (9), R60.

36. Shannon, P.; Markiel, A.; Ozier, O.; Baliga, N. S.; Wang, J. T.; Ramage, D.; Amin, N.; Schwikowski, B.; Ideker, T., Cytoscape: a software environment for integrated models of biomolecular interaction networks. *Genome research* **2003,** *13* (11), 2498-2504.

37. Chin, C.-H.; Chen, S.-H.; Wu, H.-H.; Ho, C.-W.; Ko, M.-T.; Lin, C.-Y., cytoHubba: identifying hub objects and sub-networks from complex interactome. *BMC systems biology* **2014,** *8* (S4), S11.

38. Pace, C. N.; Fu, H.; Lee Fryar, K.; Landua, J.; Trevino, S. R.; Schell, D.; Thurlkill, R. L.; Imura, S.; Scholtz, J. M.; Gajiwala, K., Contribution of hydrogen bonds to protein stability. *Protein Science* **2014,** *23* (5), 652-661.

39. Huang, C.; Wang, Y.; Li, X.; Ren, L.; Zhao, J.; Hu, Y.; Zhang, L.; Fan, G.; Xu, J.; Gu, X., Clinical features of patients infected with 2019 novel coronavirus in Wuhan, China. *The Lancet* **2020,** *395* (10223), 497-506.

40. Prompetchara, E.; Ketloy, C.; Palaga, T., Immune responses in COVID-19 and potential vaccines: Lessons learned from SARS and MERS epidemic. *Asian Pacific J. allergy Immunol* **2020,** *10*.

41. Lee, S.; Chen, T. T.; Barber, C. L.; Jordan, M. C.; Murdock, J.; Desai, S.; Ferrara, N.; Nagy, A.; Roos, K. P.; Iruela-Arispe, M. L., Autocrine VEGF signaling is required for vascular homeostasis. *Cell* **2007,** *130* (4), 691-703.

42. Vabulas, R. M.; Ahmad-Nejad, P.; da Costa, C.; Miethke, T.; Kirschning, C. J.; Häcker, H.; Wagner, H., Endocytosed HSP60s use toll-like receptor 2 (TLR2) and TLR4 to activate the toll/interleukin-1 receptor signaling pathway in innate immune cells. *Journal of Biological Chemistry* **2001,** *276* (33), 31332-31339.

43. Sauer, S.; Bruno, L.; Hertweck, A.; Finlay, D.; Leleu, M.; Spivakov, M.; Knight, Z. A.; Cobb, B. S.; Cantrell, D.; O'Connor, E., T cell receptor signaling controls Foxp3 expression via PI3K, Akt, and mTOR. *Proceedings of the National Academy of Sciences* **2008,** *105* (22), 7797-7802.

44. Kawakami, Y.; Yao, L.; Miura, T.; Tsukada, S.; Witte, O. N.; Kawakami, T., Tyrosine phosphorylation and activation of Bruton tyrosine kinase upon Fc epsilon RI cross-linking. *Molecular and cellular biology* **1994,** *14* (8), 5108-5113.

45. Stevenson, F. K.; Krysov, S.; Davies, A. J.; Steele, A. J.; Packham, G., B-cell receptor signaling in chronic lymphocytic leukemia. *Blood, The Journal of the American Society of Hematology* **2011,** *118* (16), 4313-4320.

46. Olayioye, M. A.; Neve, R. M.; Lane, H. A.; Hynes, N. E., The ErbB signaling network: receptor heterodimerization in development and cancer. *The EMBO journal* **2000,** *19* (13), 3159-3167.

47. Ayroldi, E.; Cannarile, L.; Migliorati, G.; Nocentini, G.; Delfino, D. V.; Riccardi, C., Mechanisms of the anti-inflammatory effects of glucocorticoids: genomic and nongenomic interference with MAPK signaling pathways. *The FASEB Journal* **2012,** *26* (12), 4805-4820.

48. Ishido, S.; Choi, J.-K.; Lee, B.-S.; Wang, C.; DeMaria, M.; Johnson, R. P.; Cohen, G. B.; Jung, J. U., Inhibition of natural killer cell–mediated cytotoxicity by Kaposi's sarcoma–associated herpesvirus K5 protein. *Immunity* **2000,** *13* (3), 365-374.

49. Rawlings, J. S.; Rosler, K. M.; Harrison, D. A., The JAK/STAT signaling pathway. *Journal of cell science* **2004,** *117* (8), 1281-1283.

50. Amara, U.; Flierl, M. A.; Rittirsch, D.; Klos, A.; Chen, H.; Acker, B.; Brückner, U. B.; Nilsson, B.; Gebhard, F.; Lambris, J. D., Molecular intercommunication between the complement and coagulation systems. *The Journal of Immunology* **2010,** *185* (9), 5628-5636.

51. Safran, M.; Dalah, I.; Alexander, J.; Rosen, N.; Iny Stein, T.; Shmoish, M.; Nativ, N.; Bahir, I.; Doniger, T.; Krug, H., GeneCards Version 3: the human gene integrator. *Database* **2010,** *2010*.

52. Levi, M.; Keller, T. T.; van Gorp, E.; ten Cate, H., Infection and inflammation and the coagulation system. *Cardiovascular research* **2003,** *60* (1), 26-39.

53. Lin, S.-K.; Tsai, Y.-T.; Lo, P.-C.; Lai, J.-N., Traditional Chinese medicine therapy decreases the pneumonia risk in patients with dementia. *Medicine* **2016,** *95* (37).

54. Peng, X.-q.; Zhou, H.-f.; Lu, Y.-y.; Chen, J.-k.; Wan, H.-t.; Zhang, Y.-y., Protective effects of Yinhuapinggan granule on mice with influenza viral pneumonia. *International immunopharmacology* **2016,** *30*, 85-93.

55. Dai, J.-P.; Wang, Q.-W.; Su, Y.; Gu, L.-M.; Zhao, Y.; Chen, X.-X.; Chen, C.; Li, W.-Z.; Wang, G.-F.; Li, K.-S., Emodin inhibition of influenza A virus replication and influenza viral pneumonia via the Nrf2, TLR4, p38/JNK and NF-kappaB pathways. *Molecules* **2017,** *22* (10), 1754.

56. Ding, J.; Liu, Q., Toll-like receptor 4: A promising therapeutic target for pneumonia caused by Gram-negative bacteria. *Journal of cellular and molecular medicine* **2019,** *23* (9), 5868-5875.

57. Zhang, J.; Liu, A.; Hou, R.; Zhang, J.; Jia, X.; Jiang, W.; Chen, J., Salidroside protects cardiomyocyte against hypoxia-induced death: A HIF-1α-activated and VEGF-mediated pathway. *European Journal of Pharmacology* **2009,** *607* (1-3), 6-14.

58. Sharma, N.; Mishra, K.; Ganju, L., Salidroside exhibits anti-dengue virus activity by upregulating host innate immune factors. *Archives of virology* **2016,** *161* (12), 3331-3344.

59. Huh, J.-E.; Lee, W. I.; Kang, J. W.; Nam, D.; Choi, D.-Y.; Park, D.-S.; Lee, S. H.; Lee, J.-D., Formononetin attenuates osteoclastogenesis via suppressing the RANKL-induced activation of NF-κB, c-Fos, and nuclear factor of activated T-cells cytoplasmic 1 signaling pathway. *Journal of natural products* **2014,** *77* (11), 2423-2431.

60. Moghbelinejad, S.; Nassiri-Asl, M.; Farivar, T. N.; Abbasi, E.; Sheikhi, M.; Taghiloo, M.; Farsad, F.; Samimi, A.; Hajiali, F., Rutin activates the MAPK pathway and BDNF gene expression on beta-amyloid induced neurotoxicity in rats. *Toxicology letters* **2014,** *224* (1), 108-113.

61. Nafees, S.; Rashid, S.; Ali, N.; Sultana, S., Rutin Ameliorates Cyclophosphamide Induced Oxidative Stress and Inflammation in Wistar Rats: Role of NFκB/MAPK Pathway. *Free Radical Biology and Medicine* **2014,** (76), S151.

62. Wang, P.; He, Q.; Zhu, J., Emodin-8-O-glucuronic acid, from the traditional Chinese medicine qinghuobaiduyin, affects the secretion of inflammatory cytokines in LPS-stimulated raw 264.7 cells via HSP70. *Molecular medicine reports* **2016,** *14* (3), 2368-2372.

Table 1. The docking scores of LQF components and Lopinavir with main protease of SARS-CoV-2

number	components	docking score (kcal/mol)
1	Rutin	-9.1
2	Hyperoside	-9.0
3	Forsythoside E	-8.7
4	Liquiritin apioside	-8.6
5	Emodin	-8.3
6	Chlorogenic acid	-7.9
7	Amygdalin	-7.8
8	Cryptochlorogenic acid	-7.6
9	Lopinavir	-7.6
10	Isoliquiritin apioside	-7.5
11	Neochlorogenic acid	-7.4
12	Chrysophanol 8-O-glucoside	-7.2
13	Rhein	-7.2
14	Isoliquiritin	-7.1
15	Emodin 8-O-β-D-glucoside	-7.1
16	Sweroside	-7.0
17	Formononetin	-7.0
18	Salidroside	-6.9
19	Liquiritigenin	-6.9
20	Loganic acid	-6.6
21	Secologanin	-5.9
1′	Lopinavir	-7.3

Table 2. Information of the main effective component in LQF-viral pneumonia related targets-pathways of anti-inflammatory and immunity in network

pathway	[a]count	[b]function	Main ingredients (target counts)
VEGF signaling pathway	14	Other	Salidroside (1) Loganic acid (1) Amygdalin (2) Sweroside (1) Emodin 8-O-β-D-glucoside (2) Chrysophanol 8-O-glucoside (1) Formononetin (2) Chlorogenic acid (2) Hyperoside (2)
Toll-like receptor signaling pathway	9	Inflammation & immunity	Amygdalin (1) Emodin 8-O-β-D-glucoside (1) Formononetin (2) Chlorogenic acid (2) Rutin (2) Hyperoside (1)
T cell receptor signaling pathway	8	Immunity	Amygdalin (1) Emodin 8-O-β-D-glucoside (1) Chlorogenic acid (4) Rutin (1) Hyperoside (1)
Fc epsilon RI signaling pathway	7	Inflammation	Amygdalin (1) Emodin 8-O-β-D-glucoside (1) Formononetin (2) Chlorogenic acid (1) Rutin (1) Hyperoside (1)
B Cell Receptor Signaling pathway	7	Immunity	Amygdalin (1) Emodin 8-O-β-D-glucoside (1) Chlorogenic acid (2) Rutin (2) Hyperoside (1)
ErbB signaling pathway	7	Inflammation	Amygdalin (1) Emodin 8-O-β-D-glucoside (1) Formononetin (2) Chlorogenic acid (2) Hyperoside (1)
MAPK signaling pathway	6	Inflammation	Formononetin (2) Chlorogenic acid (1) Rutin(3)
Natural killer cell mediated cytotoxicity	6	Immunity	Formononetin (2) Chlorogenic acid (1) Rutin (3)
JAK-STAT signaling pathway	6	Inflammation & immunity	Amygdalin (1) Emodin 8-O-β-D-glucoside (1) Formononetin (1) Chlorogenic acid (1) Rutin (1) Hyperoside (1)

Complement and coagulation cascades	2	Inflammation	Loganic acid (1) Secologanin (1) Formononetin (1) Rutin (1)

[a]signaling pathways related targets of counts.

[b]main functions of signaling pathways.

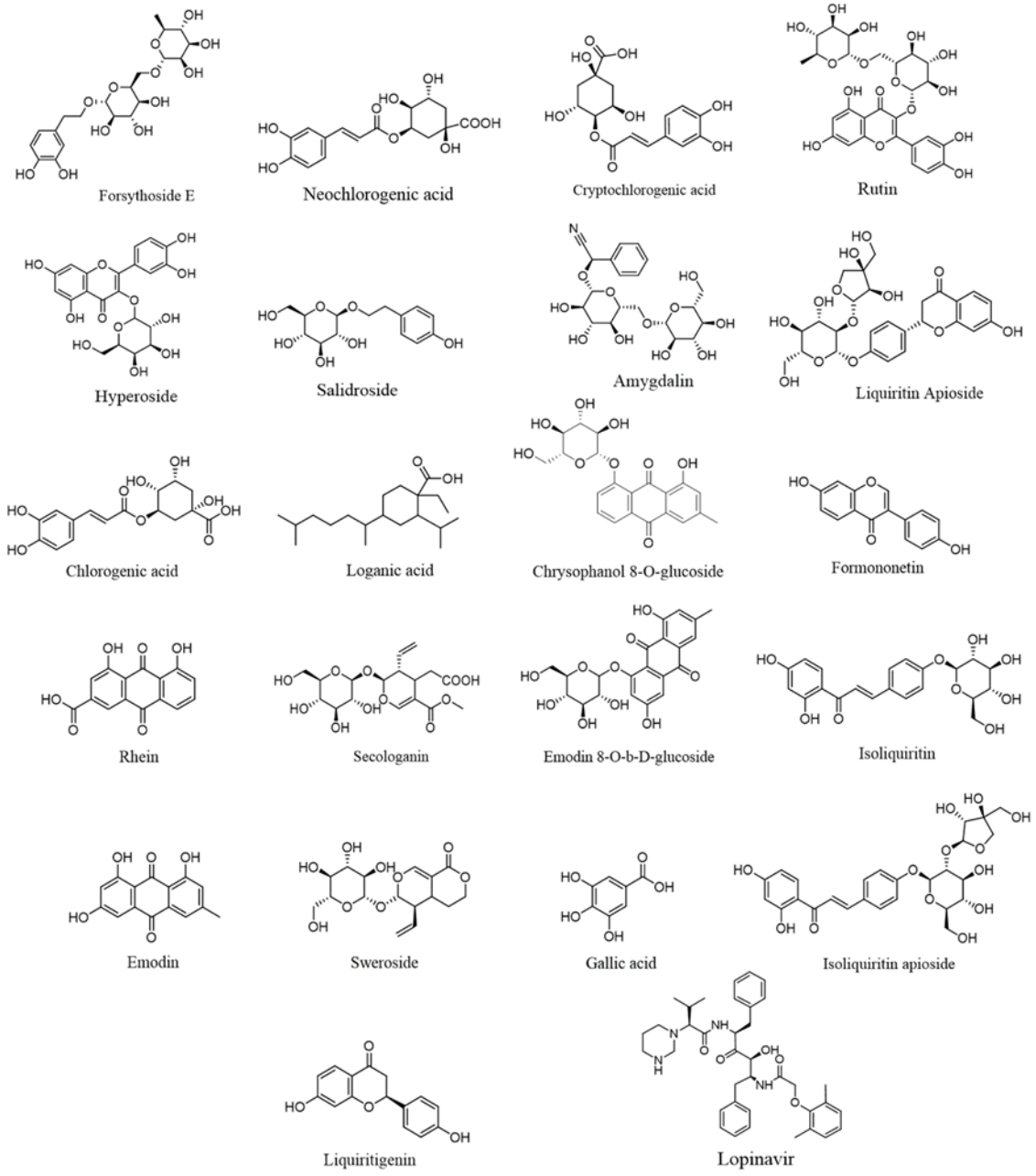

1 **Figure 1.** The schematic molecular structures of the 21 components in LQF and Lopinavir.

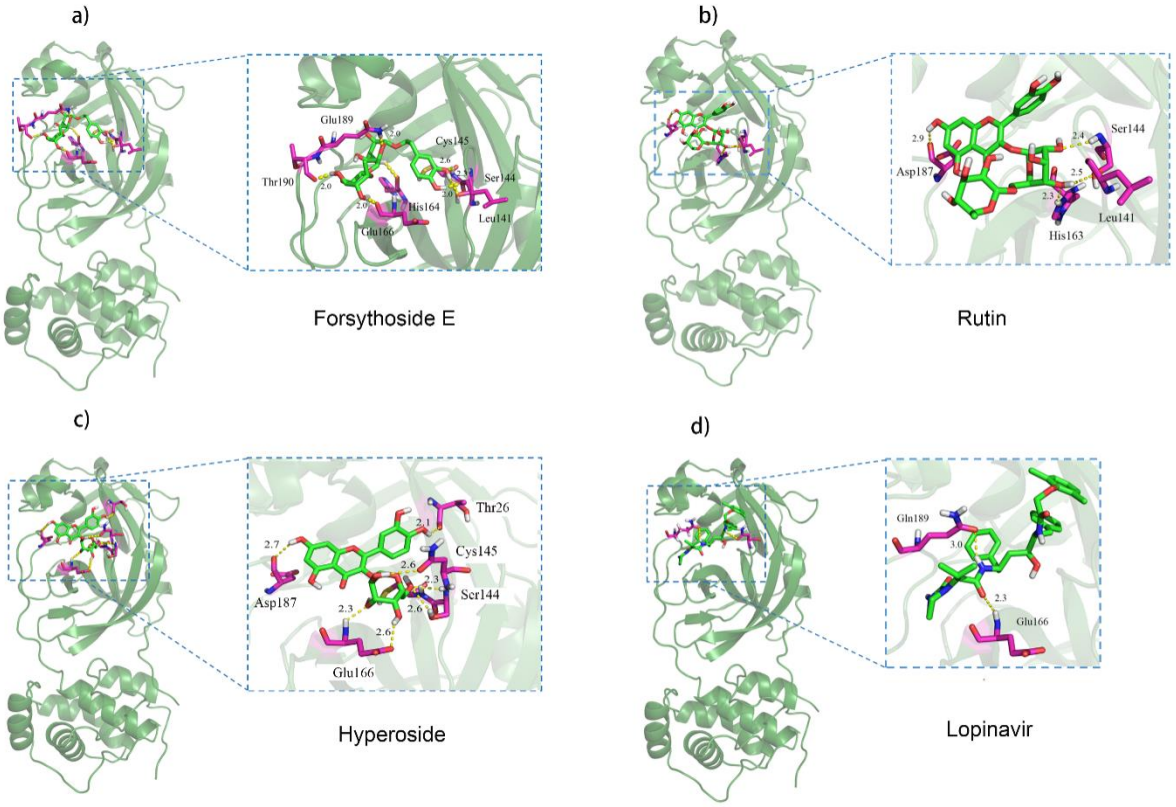

1 **Figure 2.** The optimized binding patterns of ligands with main protease by molecular docking,

2 including a) Forsythoside E; b) Rutin; c) Hyperoside; and d) Lopinavir.

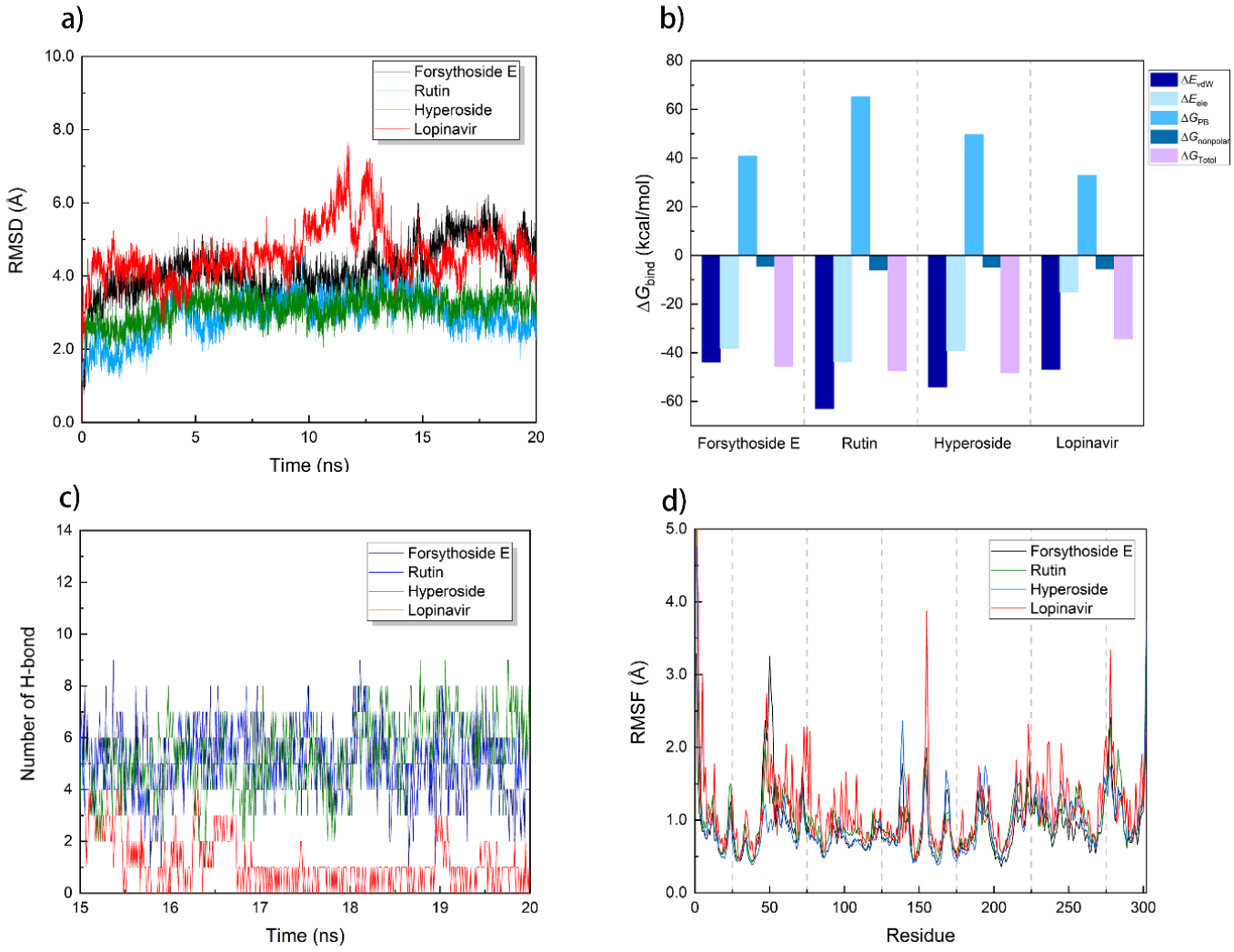

Figure 3. a) RMSD plot during molecular dynamics simulations. The lines represent RMSD between Cα atoms of protein and ligands; b) the calculated binding free energy and energy decomposition using MM/PBSA on each ligand with SARS-CoV-2 main protease; c) the number of hydrogen bond between ligands and binding pocket in SARS-CoV-2 main protease; d) RMSF differences between ligands during the last 20 ns MD simulations.

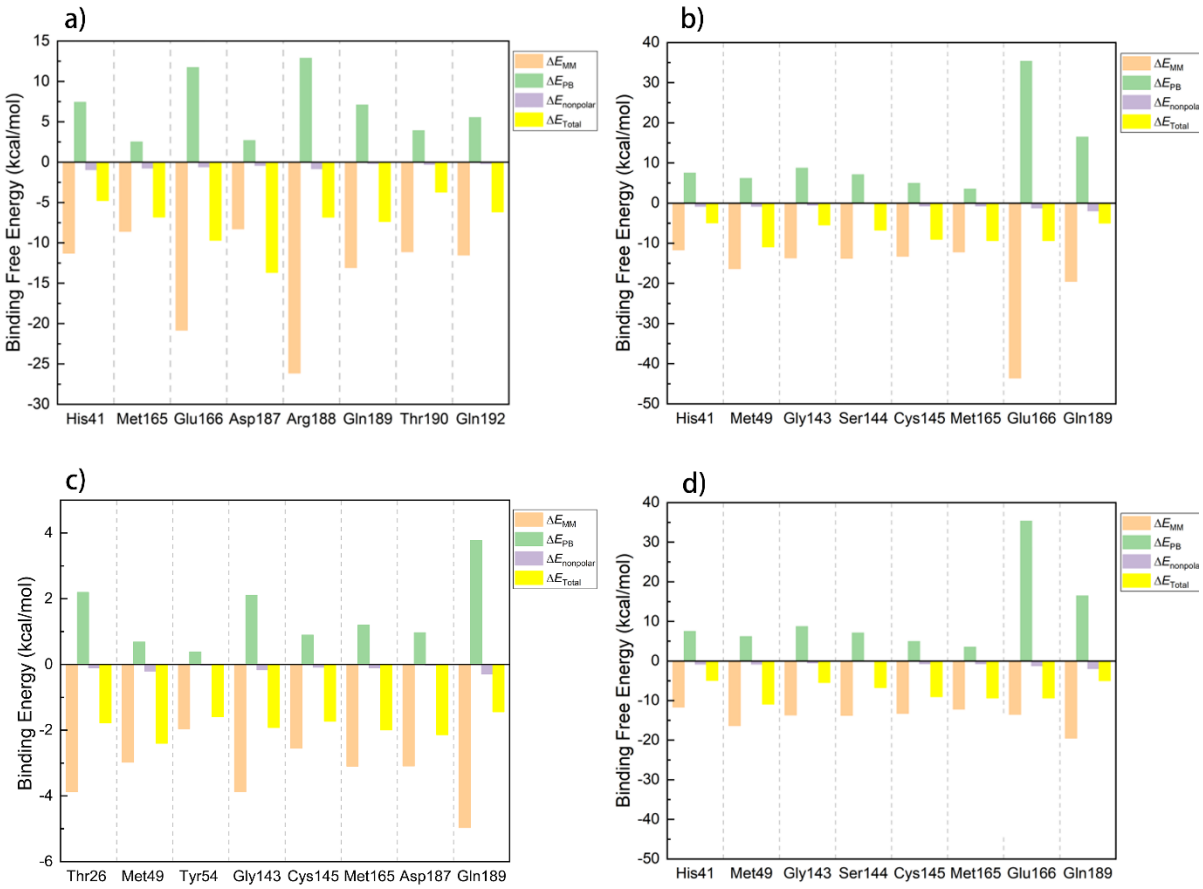

Figure 4. Decomposition of the binding energies of ligands on each residue on SARS-CoV-2 main protease. a) Forsythoside E; b) Rutin; c) Hyperoside; and d) Lopinavir.

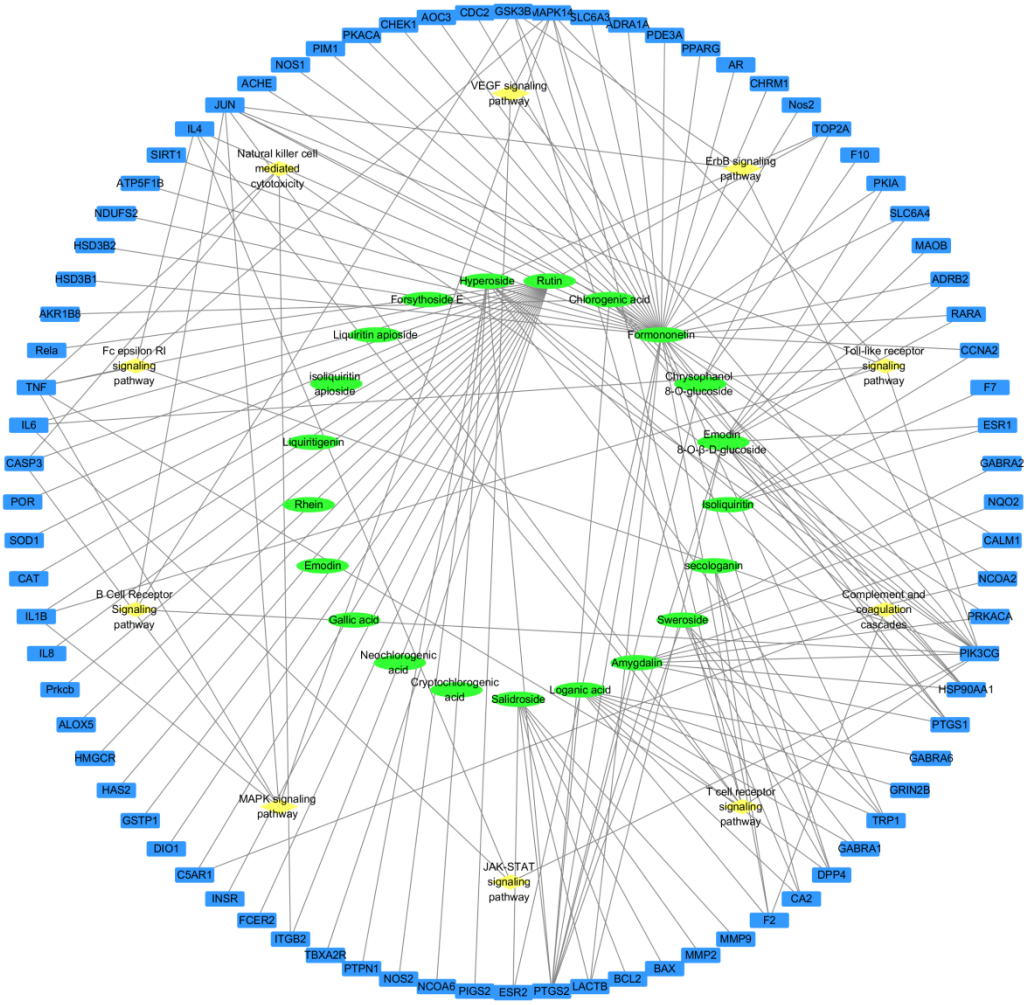

Figure 5. The plotted diagram of the main effective component in LQF-viral pneumonia related targets-pathways of anti-inflammatory and immunity. Note that green nodes represent the candidate compounds; blue nodes represent direct effective targets and predicted targets; yellow ones refer to the related pathways.